Leveraging Signals of Opportunity: Phase Tracking & Differential Correlation

Christian A. Lichtenberger[1], Florian Binder[1], and Thomas Pany[1]

[1] *University of the Bundeswehr Munich*

BIOGRAPHY

Christian A. Lichtenberger has been a research associate at the Institute for Space Technology and Space Applications (ISTA) at the University of the Bundeswehr Munich (UniBw M) since 2019. He holds a Master's degree in Geodesy and Geoinformation from the Technical University of Munich (TUM). Besides stochastic modeling of low-cost GNSS receivers and integrity analysis of safety-critical systems, his research field includes the extension of the Multi Sensor Navigation Analysis Tool (MuSNAT) for LEO-PNT signals.

Florian Binder received a master's degree in Geodesy and Geoinformation from the Technical University of Munich (TUM). He is currently working at the Institute for Space Technology and Space Applications (ISTA) at the University of the Bundeswehr Munich (UniBw M) as a research associate. His research activities include LEO-PNT, signal quality monitoring and SDR receivers.

Thomas Pany works for the University of the Bundeswehr Munich (UniBw M) as a full professor for satellite navigation since 2016. He obtained his PhD from the Graz University of Technology in 2001 and worked in the GNSS industry for seven years. He authored around 250 publications including one monography and received five best presentation awards from the ION. He is an active member of the ION and IEEE, and he also organizes the Munich Satellite Navigation Summit. His research interests are centered around navigation signal processing, including signal design and fusion with inertial navigation.

ABSTRACT

Carrier phase tracking of signals of opportunity is an active research topic with the potential to enable high-accuracy and technology-agnostic navigation using non-cooperative satellite transmitters. However, sparse and data-centric signal structures, combined with pronounced Doppler dynamics, pose severe challenges to conventional phase-locked loop (PLL) architectures.

This paper investigates carrier phase tracking of the Starlink Ku-band downlink using block-processing and differential correlation approaches. An existing PLL-based tracking framework is extended with a block-processing discriminator (BPD), enabling coherent processing over multiple epochs. The approach is first validated using simulated 5G non-terrestrial networks (NTN) signals, confirming correct carrier phase tracking behavior under controlled conditions. When applied to real Starlink measurements, however, the inherent carrier phase instability (severe phase jitter inherent to the transmission scheme) and sparse replica structure significantly degrade the robustness of undifferenced carrier phase tracking, even when using a block-processing discriminator.

To mitigate these effects, differential correlator-based tracking methods are investigated. Single-difference and double-difference processing are analyzed and experimentally evaluated using a dedicated dual-receiver measurement setup. The results demonstrate that differential processing effectively suppresses common-mode effects such as satellite-induced Doppler dynamics and enables reliable tracking of relative carrier phase variations. Single-difference tracking is shown to be feasible subject to receiver oscillator stability, while double-difference tracking further improves robustness at the cost of increased implementation complexity.

The presented findings highlight fundamental limitations of undifferenced carrier phase tracking for non-cooperative low earth orbit (LEO) communication signals such as Starlink and provide important insights into the design of robust carrier phase tracking receivers for emerging signals of opportunity.

I. INTRODUCTION

LEO satellite constellations have gained increasing attention in recent years, not only for broadband communication services but also as potential signals of opportunity (SoOP) for positioning, navigation and timing (PNT) applications. Their global coverage, high transmission power, and large available bandwidth make such signals attractive complements to traditional global navigation satellite system (GNSS), particularly in challenging environments or for enhanced robustness (Kassas et al., 2018).

Among the emerging LEO constellations, Starlink represents one of the most prominent examples. Its Ku-band downlink signals offer exceptionally large bandwidths and high received carrier-to-noise density ratios, which in principle enable highly accurate ranging and carrier phase observations. However, unlike GNSS signals, Starlink is a non-cooperative system optimized for data transmission rather than navigation. As a result, only limited and sparsely distributed portions of the signal are known and repeatable, posing significant challenges for replica-based acquisition and tracking (Soualle et al., 2024, 2025).

Carrier phase tracking is of particular interest, as it enables high-precision observables that are essential for advanced PNT concepts such as precise positioning, relative navigation, or attitude determination. At the same time, it is especially sensitive to signal impairments. For Starlink and similar LEO SoOP, carrier phase tracking is challenged by a combination of sparse replica availability, poor stability clocks, high Doppler shifts and Doppler rates, and time-varying signal content. Conventional PLL designs, which rely on continuous and energy-rich correlation outputs, often exhibit unstable behavior or fail to maintain lock under these conditions (Kozhaya et al., 2024a, 2025).

To address these challenges, alternative tracking strategies that depart from classical sample-wise discriminator concepts are required. One promising approach is block-processing, in which multiple consecutive tracking epochs are coherently combined to increase the effective integration time and accumulate sufficient signal energy. Another approach exploits differential processing, where relative carrier phase variations between multiple receivers are tracked, thereby mitigating common-mode effects such as satellite-induced Doppler dynamics.

This paper investigates carrier phase tracking of Starlink downlink signals using two complementary approaches: a block-processing-based delay-, frequency- and phase-locked loop and a differential correlator-based tracking method. The block-processing approach is validated using both simulated 5G NTN signals and real Starlink measurements, demonstrating its ability to achieve stable carrier phase tracking despite sparse replica structures. The differential approach is evaluated using a dedicated measurement setup with controlled relative motion between two receivers, enabling direct assessment of relative carrier phase tracking performance.

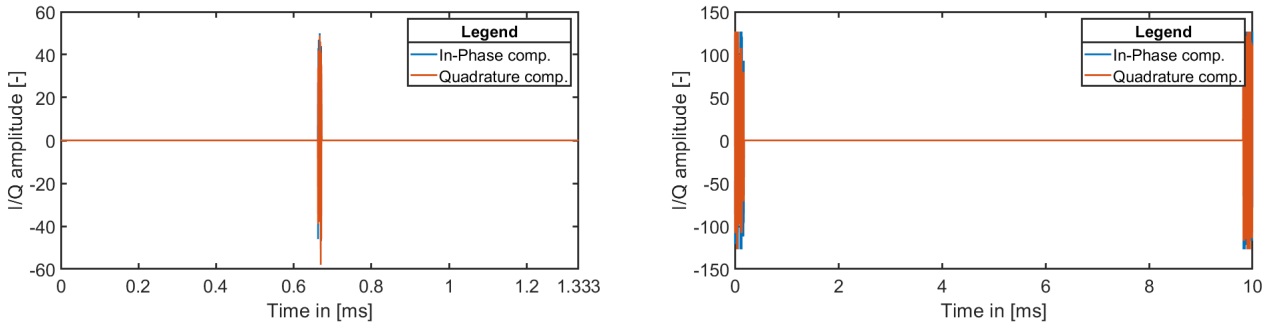
The remainder of this paper is organized as follows. Section II describes the relevant signal characteristics and outlines the fundamental challenges associated with carrier phase tracking of sparse LEO signals. Section III introduces the block-processing-based tracking approach. Section IV presents the differential correlator formulation, followed by a description of the measurement setup in Section V. Tracking results obtained from simulations and real measurements are presented and discussed in Section VI and Section VII, respectively. Finally, conclusions and perspectives for future work are given in Section VIII.

II. SIGNAL CHARACTERISTICS AND TRACKING CHALLENGES

The feasibility of carrier phase tracking using non-cooperative LEO communication signals is fundamentally constrained by the signal structure and its temporal characteristics. In contrast to navigation signals with well-defined and continuously available spreading codes, SoOP such as Starlink are primarily optimized for data transmission rather than precise synchronization or tracking. As a result, only limited portions of the signal can be exploited to generate a replica suitable for coherent processing.

The Starlink Ku-band downlink signal consists of up to eight channels with a bandwidth of 240 MHz each, separated by guard bands. Due to the dynamic network allocation, the number of active channels varies depending on traffic demand within a given service (hexa-)cell. The network configuration remains constant over short intervals, referred to as fixed assignment intervals (FAIs), with a duration of approximately 15 s. While the overall signal structure has been reverse-engineered in recent years, only a small subset of the transmitted symbols is currently suitable for replica generation (Qin et al., 2024, 2025).

Each channel is based on an orthogonal frequency-division multiplexing (OFDM) waveform with 1,024 subcarriers, resulting in a subcarrier spacing of 234.375 kHz. A frame consists of 302 OFDM symbols, of which only two synchronization symbols — the primary synchronization sequence (PSS) and the secondary synchronization sequence (SSS) — are known and repeatable. These symbols appear at the beginning of each frame and span the full channel bandwidth. All remaining symbols contain user data or unknown synchronization patterns and therefore cannot be exploited for coherent correlation-based tracking. Consequently, only approximately 0.66 % of the frame duration contributes usable signal energy for replica-based processing (Humphreys et al., 2023; Komodromos and Humphreys, 2025).



(a) Starlink PSS/SSS replica signal in time domain

(b) 5G NTN positioning reference signal (PRS) replica signal in time domain

Figure 1: Visualization of replica signals in time domain

Figure 1a illustrates the resulting replica signal in the time domain. The sparse structure, characterized by long intervals of zero-valued samples, leads to a severely reduced correlation energy. In combination with the high Doppler dynamics inherent to LEO satellites, this sparsity poses a major challenge for stable carrier phase tracking. Even small residual frequency errors or carrier phase noise can lead to rapid decorrelation, causing conventional tracking loops to lose lock.

In addition to the limited replica availability, the Starlink signal is subject to large Doppler shifts and Doppler rates, which further complicate coherent tracking. The high orbital velocity results in significantly increased dynamic stress on the receiver compared to typical GNSS or terrestrial communication systems. As a consequence, classical PLL or frequency-locked loop (FLL) designs, which rely on continuous and energy-rich correlation outputs, often require substantially increased loop bandwidths or higher-order filter structures in order to maintain stable tracking.

To further investigate carrier phase tracking under sparse signal conditions, a simulated 5G NTN signal is considered in this work, see Soualle et al. (2025) for PRS configuration and the simulation toolchain. Similar to the Starlink signal, the 5G NTN downlink waveform exhibits a highly sparse structure, as only the PRS symbols are known and available for replica generation, while the remaining frame content carries user data or may not be exploitable by the user reliably (see Figure 1b). As a result, the effective replica occupancy is comparably low, leading to similar limitations in correlation energy and tracking robustness. The use of a simulated 5G NTN signal enables controlled validation of the proposed tracking approaches under LEO-like Doppler dynamics, while preserving the fundamental challenge of sparse replica availability (Binder et al., 2026; 3GPP, 2022).

The severe limitation in usable signal energy motivates the investigation of alternative carrier phase tracking strategies that depart from classical sample-wise discriminator designs. In the following sections, two such approaches are investigated: a block-processing discriminator, and a differential correlator-based tracking method. Both approaches aim to improve robustness against sparse replicas and high Doppler dynamics, enabling stable carrier phase tracking even when only band-limited PSS/SSS symbols are available.

III. BLOCK-PROCESSING DISCRIMINATOR

The block-processing-based tracking approach employed in this work was originally introduced and described in detail in (Lichtenberger et al., 2025). In the following, only the key concepts required to understand its application to carrier phase tracking of sparse LEO signals are summarized. For a full mathematical treatment, the reader is referred to the original publication.

The core idea of the BPD is to increase the effective coherent integration time by jointly processing multiple consecutive tracking epochs. Instead of relying on the correlation output of a single frame, a batch of N epochs is coherently combined, each with a duration of one OFDM frame, allowing the accumulation of signal energy that would otherwise be insufficient for stable tracking. This approach is particularly well suited for sparse signals such as Starlink and 5G NTN, where only a small pulse of the transmitted frame can be exploited for replica-based correlation.

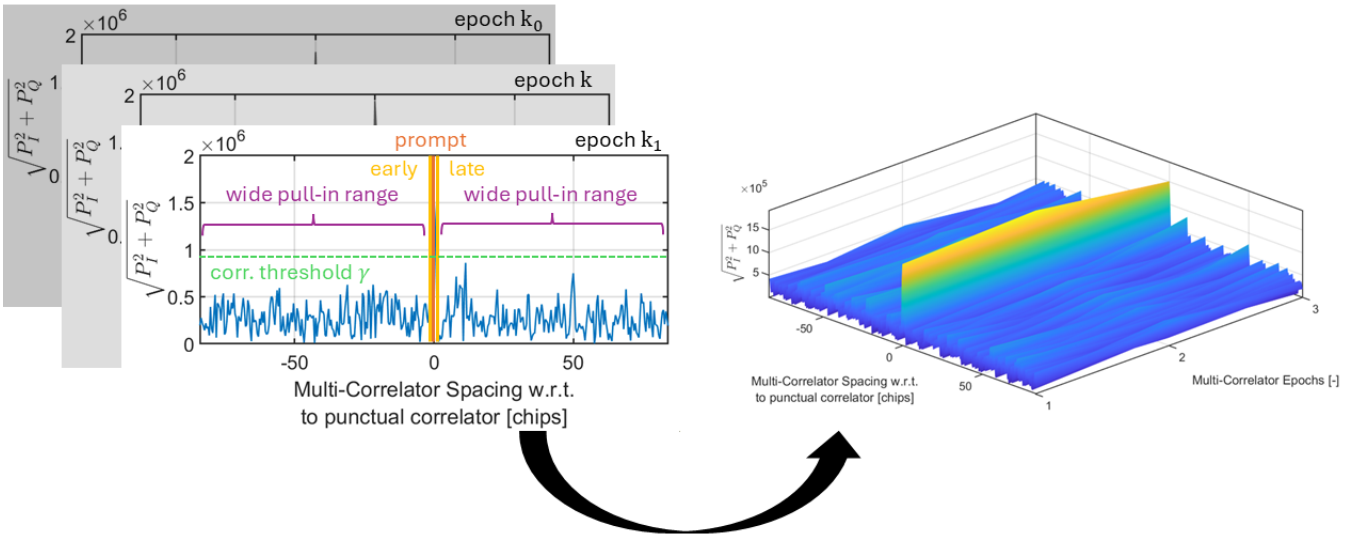


Figure 2: Collection of consecutive multi-correlator epochs

To enable robust pull-in under large initial code phase and frequency errors, a dense multi-correlator architecture is employed. A large number of correlator points, symmetrically distributed around the prompt position, provides a wide search range in code phase. This significantly exceeds the pull-in range of classical early–prompt–late structures and ensures reliable acquisition and re-acquisition under high Doppler dynamics (see Figure 2).

$$n_{max}, f_{max} = \arg\max_{n,f} \left[\sum_{k=k_0}^{k_1} C_n(t_k) \cdot e^{-2\pi f(t_k - t_m)} \right] \tag{1}$$

The algorithm operates in two modes: a wide-range mode and a narrow-range mode. In wide-range mode, batches of correlator outputs are collected and evaluated jointly in a two-dimensional code phase–frequency search space (see Figure 3 and refer to Equation (1)). The location of the global maximum is estimated using a maximum likelihood criterion, directly yielding discriminator values for code phase, frequency, and now also carrier phase. Once the prompt correlator approaches the global maximum (refer to Equation (2)), exceeding threshold γ_p, the algorithm transitions to narrow-range mode, in which conventional tracking loop discriminators are used.

$$\frac{|\overline{C}_{n_{max}}|}{|\overline{C}_{n_p}|} > \gamma_p \tag{2}$$

In narrow-range mode, the discriminator outputs are computed from the coherently integrated correlator values as

$$\begin{aligned} e_D &= \alpha \frac{|\overline{C}_{n_e}| - |\overline{C}_{n_l}|}{|\overline{C}_{n_p}|} && \text{(code phase)} \\ e_F &= \Re\left\{ \frac{\overline{F}_{n_p} \cdot N}{2\pi i \cdot \overline{C}_{n_p} \cdot \kappa} \right\} && \text{(frequency)} \\ e_P &= \arg\left\{ \overline{C}_{n_p} \right\} \cdot \frac{1}{2\pi} && \text{(carrier phase)} \end{aligned} \tag{3}$$

where $\overline{C}_{n_e}$, $\overline{C}_{n_p}$, and $\overline{C}_{n_l}$ denote the coherently integrated early, prompt, and late correlator values, respectively. The F-correlator $\overline{F}_{n_p}$ represents the time-weighted sum of prompt correlator values over the batch interval and enables frequency estimation based on the linearized phase evolution.

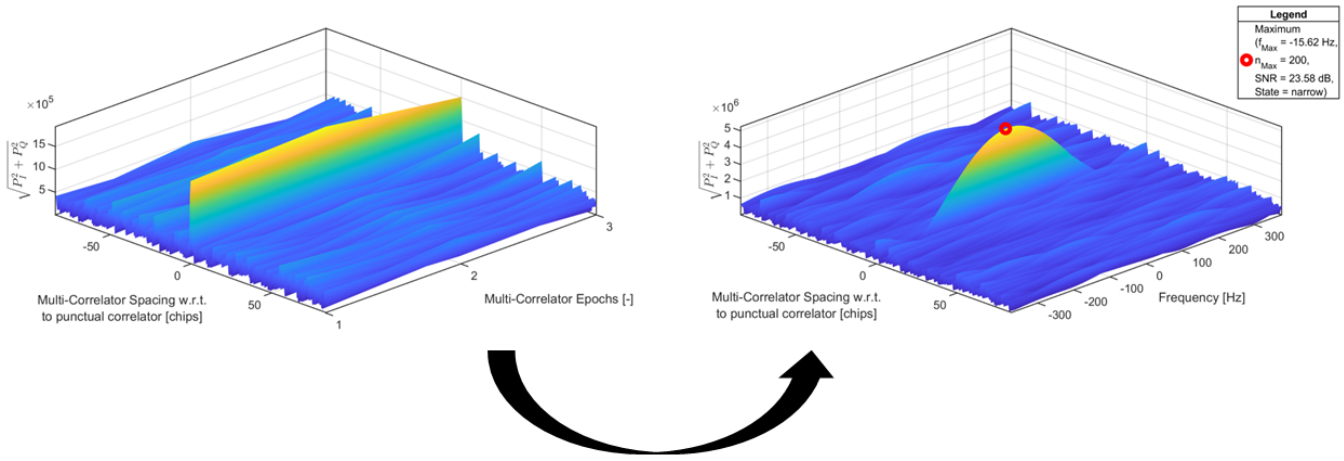


Figure 3: Transformation of series of multi-correlator epochs to frequency domain

In wide-range mode, the discriminator values for code phase and frequency are obtained directly from the estimated maximum of the two-dimensional search space, while the carrier phase discriminator uses the found maximum correlator value instead of the prompt correlator value:

$$\begin{aligned} e_D &= \tau_{n_{max}} && \text{(code phase)} \\ e_F &= f_{max} && \text{(frequency)} \\ e_P &= \arg\left\{ \overline{C}_{n_{max}} \right\} \cdot \frac{1}{2\pi} && \text{(carrier phase)} \end{aligned} \tag{4}$$

For carrier phase tracking, a second-order FLL-aided third-order PLL architecture is employed. In the Starlink case, additional aiding of the delay-locked loop (DLL) is not applied, since the code and carrier estimates can diverge due to the sparse replica structure and time-varying signal content, which leads to unstable delay tracking (this behavior is discussed in Section VII). In contrast, first order narrow bandwidth DLL carrier aiding is feasible for the simulated 5G NTN signal, and was evaluated as part of the validation experiments. In addition to the aided configuration, the simulation study also includes an unaided scenario, i.e., a stand-alone operation of DLL, FLL, and PLL, to isolate the benefit of loop aiding under controlled conditions. Unless stated otherwise, the filter bandwidths used for Starlink carrier phase tracking are: DLL 20 Hz (2nd-order, without aiding), FLL 50 Hz (2nd-order), and PLL 40 Hz (3rd-order).

The performance of the block-processing-based FLL/PLL approach is evaluated in Section VI and Section VII using both simulated 5G NTN signals and real Starlink measurements.

IV. DIFFERENTIAL CORRELATOR

As demonstrated in the previous sections and by other works from Kozhaya et al. (2025) Starlink signals may suffer from the fact that the carrier phase varies from frame to frame, due to various reasons which are, however, difficult to guess for an opportunistic user. In previous publications like (Pany et al., 2012; Pany, 2010) a certain form of processing correlator values has been introduced - namely difference correlators - that eliminates these phase variations by forming single or double differences of correlator values. This concept shall be recapitulated here. It has also be noted that other signal processing methods use the term 'difference correlators'. Their target use case differs substantially from that considered in this work and primarily addresses signal acquisition, signal power estimation, or efficient computation of multi-correlator outputs.

1. Prompt Correlator and Carrier Phase

To introduce the concept of difference correlators, we first recapitulate carrier phase tracking inside the navigation receiver. The received signal is governed by a true but unknown carrier phase, which is denoted by ϕ (if expressed in radians) or by Φ if expressed in meters. The navigation receiver aligns a replica signal to the received signal, and the phase of the replica signal is denoted by $\hat{\phi}$ or $\hat{\Phi}$, respectively. The replica phase $\hat{\phi}$ is part of the carrier numerically controlled oscillator (NCO) values together with the Doppler shift. The replica phase furthermore defines the value output to the navigation processing or to the receiver independent exchange format (RINEX) file.

To track the carrier phase, the prompt correlator values P are utilized. They measure the misalignment between the replica and received carrier phase, i.e.

$$P \simeq \exp\left\{j\left(\phi - \hat{\phi}\right)\right\} + \text{noise}. \tag{5}$$

The symbol '$\simeq$' denotes proportionality, which we use here to indicate that we are focusing solely on the carrier phase relation and ignore the signal amplitude or effects related to code misalignment. Using Equation (5), we define a so-called raw correlator value R as

$$R = P \exp\left\{j\hat{\phi}\right\}, \tag{6}$$

and

$$R \simeq \exp\{j\phi\} + \text{noise} \tag{7}$$

is thus directly proportional to the exponential of the true signal phase. It should be noted that R is not impacted by the carrier phase tracking scheme employed to obtain $\hat{\phi}$, as its impact is removed when computing Equation (6). Thus, it can be applied to standard DLL/FLL/PLL tracking, vector tracking, or to an architecture where channels share the same NCO (master/slave architecture).

2. Single- and Double-Differences

It is well known from real time kinematic (RTK) positioning that receiver single-differencing removes satellite specific delays from code/carrier observations and double-differencing removes furthermore receiver specific delays. To define a consistent terminology, those processes are recapitulated here referring to the indexing scheme of Figure 4.

A carrier phase observations Φ_m^k for satellite k and receiver m is modeled as

$$\Phi_m^k = N_m^k \lambda + b^k + \rho_m^k + c\left(dt_s^k - dt_{r;m}\right) + I_m^k + T_m^k + \epsilon_m^k \tag{8}$$

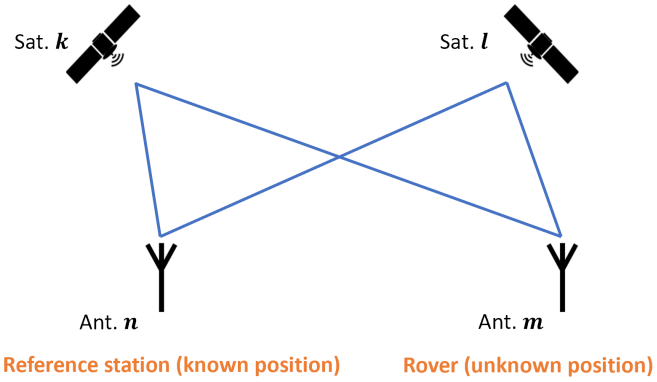


Figure 4: Visualization of single/double differencing

with $\rho_m^k = \| \mathbf{x}^k - \mathbf{x}_m \|$. The carrier ambiguity is denoted as N, the wavelength as λ, the satellite/receiver positions as $\mathbf{x}^k/\mathbf{x}_m$, the geometric distance as ρ, the satellite/receiver clock error as dt_s/dt_r, the ionospheric/tropospheric delay as I/T and any measurement errors as ϵ.

The receiver single difference is defined as

$$\Phi_{m,n}^k = \Phi_m^k - \Phi_n^k = N_{m,n}^k \lambda + \rho_{m,n}^k - c dt_{r;m,n} + \epsilon_{m,n}^k, \tag{9}$$

and the double difference as

$$\Phi_{m,n}^{k,l} = \Phi_{m,n}^k - \Phi_{m,n}^l = N_{m,n}^{k,l} \lambda + \rho_{m,n}^{k,l} + \epsilon_{m,n}^{k,l}. \tag{10}$$

We use the notation that a pair of indices indicates the difference between two receiver or between two satellites.

3. Difference Correlators

Due to the relationship defined via Equations (7), we can transfer single- and double differencing to the correlator level. The single-difference correlator $R_{m,n}^k$ is given by

$$R_{m,n}^k = R_m^k \overline{R_n^k} \simeq \exp\left\{ j\phi_{m,n}^k \right\} + \text{noise}, \tag{11}$$

and the double-difference correlator $R_{m,n}^{k,l}$ by

$$R_{m,n}^{k,l} = R_{m,n}^k \overline{R_{m,n}^l} = R_m^k \overline{R_n^k R_m^l} R_n^l \simeq \exp\left\{ j\phi_{m,n}^{k,l} \right\} + \text{noise}, \tag{12}$$

where $\bar{\cdot}$ denotes the operation of complex conjugation.

Single difference correlator values are independent of any satellite specific phase biases and this includes frame specific phase variations as discussed before. Double difference values are independent of any receiver phase biases and this includes local clock/local oscillator jitter that can be significant to the high carrier frequency.

4. Assumptions

Within this work we make the following assumptions to simplify the discussion. They are:

- Short baseline for synchronous measurements at rover/reference
- Double differencing assumptions
- Insignificant multipath

a) Short Baseline

Within our software receiver, correlator values are computed at the end of a frame period, i.e. every 4/3 milliseconds for Starlink. If the reference station and rover are separated by large distances, these epochs would not be synchronous. The impact of this has not yet been investigated, and thus we simply assume that the baseline is short and the impact can be neglected.

With the baseline denoted as $\Delta\mathbf{x} = \mathbf{x}^m - \mathbf{x}_n$ the single/double difference geometric distance is given for this short-baseline assumption as

$$\rho^k_{m,n} \simeq \left(\mathbf{e}^k_m\right)^\top \Delta\mathbf{x}; \quad \rho^{k,l}_{m,n} \simeq \left(\mathbf{e}^k_m - \mathbf{e}^l_m\right)^\top \Delta\mathbf{x} \tag{13}$$

where $\mathbf{e}^k_m = \left(\mathbf{x}^k - \mathbf{x}_m\right)/\rho^k_m$ denotes the unit vector from the receiver m to the satellite k.

b) Double Differencing Assumptions

Within this work some further assumptions are made to conduct double differencing.

First, it is noted that the difference correlator values have to be formed at the satellite sent time scale (i.e. correlator values belonging to the same frame are multiplied with each other). Since the broadcasting of frames from different satellites is not strictly synchronized and since the travel time from different satellites to the user is different, receiver specific parameters (clock error, position) might slightly vary between the reception epochs of the frames from the two different satellites. This variation is neglected in this work, but can (most likely) be accurately modeled if sufficient effort is invested.

Second, in our data sets we achieved simultaneous reception of two Starlink satellites only on two different frequencies (this is expected, although Kozhaya et al. (2024b) reports that Starlink uses polarization diversity as well, which would allow to receive two satellites on the same frequency with different polarizations). When forming double-differenced correlator values via Equation (12) the double-differenced carrier phase is expressed in radians, results in

$$\phi^{k,l}_{m,n} = \phi^k_{m,n} - \phi^l_{m,n} = 2\pi N^k_{m,n} + 2\pi/\lambda_k \left(\rho^k_{m,n} - cdt_{r;m,n}\right) - 2\pi N^l_{m,n} - 2\pi/\lambda_l \left(\rho^l_{m,n} - cdt_{r;m,n}\right) + \text{noise} \tag{14}$$

with λ_k and λ_l being the slightly different wavelengths. Merging observations at different frequencies has been discussed long time ago already for GLONASS by e.g. Roßbach (2001), and has now been reinvestigated for signals of opportunity by e.g. Yang et al. (2025). A possible way to handle different frequencies exists, if the frequencies are a multiple of a base frequencies, or stated differently if there exists a wavelength λ_0 such that $\lambda_k = K\lambda_0$ and $\lambda_l = L\lambda_0$ with K, L being integers. Then it is possible to model a modified double-differenced phase $\tilde{\phi}^{k,l}_{m,n}$ in radians as

$$\tilde{\phi}^{k,l}_{m,n} = K\phi^k_{m,n} - L\phi^l_{m,n} = 2\pi\left(KN^k_{m,n} - LN^l_{m,n}\right) + 2\pi/\lambda_0\rho^{k,l}_{m,n} + \text{noise} \tag{15}$$

and resulting in modified double-differenced correltor values as

$$\tilde{R}^{k,l}_{m,n} = \left(R^k_{m,n}\right)^K \left(\overline{R^l_{m,n}}\right)^L = \exp\left\{\tilde{\phi}^{k,l}_{m,n}\right\} + \text{noise}. \tag{16}$$

Whereas this approach is theoretically feasible, the resulting wavelength λ_0 is extremely small and the practical use of Equation (16) is doubtful as the noise exceeds the wavelength by far.

A slightly more practical use of double-difference carrier phase observations may results if the time-difference is additionally employed (so-called delta-range observation). If Δ denotes the time difference between two epochs, then

$$\Delta\phi^{k,l}_{m,n} = 2\pi(\bar{f} + \delta f_k)/c\left(\Delta\rho^k_{m,n} - c\Delta dt_{r;m,n}\right) - 2\pi(\bar{f} + \delta f_l)/c\left(\Delta\rho^l_{m,n} - c\Delta dt_{r;m,n}\right) + \text{noise} \tag{17}$$

where we assume that the ambiguities remain constant and thus cancel. The mean frequency $\bar{f} = (f_k + f_l)/2$ is introduced as well as the delta frequency such that $f_{k/l} = \bar{f} + \delta f_{k/l}$. This equation can be rewritten to

$$\Delta\phi^{k,l}_{m,n} = 2\pi\bar{f}\Delta\rho^{k,l}_{m,n} + \frac{2\pi\delta f_k}{c}\left(\Delta\rho^k_{m,n} - c\Delta dt_{r;m,n}\right) - \frac{2\pi\delta f_l}{c}\left(\Delta\rho^l_{m,n} - c\Delta dt_{r;m,n}\right) + \text{noise} \tag{18}$$

The second and third term in the equations indicates the impact of the different carrier frequencies. If the sum of these terms - converted to meters assuming the wavelength corresponding to $\bar{f}$ - is smaller than the measurement noise, it can be neglected, which is expressed as the condition

$$\frac{2\pi\delta f_k}{c}\left(\Delta\rho^k_{m,n} - c\Delta dt_{r;m,n}\right) - \frac{2\pi\delta f_l}{c}\left(\Delta\rho^l_{m,n} - c\Delta dt_{r;m,n}\right) \ll \text{noise}. \tag{19}$$

Assuming $\Delta\rho^l_{m,n} \approx \Delta\rho^k_{m,n} \approx \Delta\rho_{m,n}$ and $\Delta dt_r = 0$ then a coarse estimation of the maximum tolerable range variations results in

$$\Delta\rho_{m,n} \ll \text{noise}\frac{\bar{f}}{\delta f_k - \delta f_l}. \tag{20}$$

Assuming a 'noise' of 1 millimeter, adjacent Starlink channels (f_k=11.325 GHz and f_l=11.575 GHz) then the maximum tolerable motion $\Delta\rho_{m,n}$ is around 5 centimeter. To which extend Equation (19) is valid, might by application specific but it appears to be very tight. If not fulfilled, the double differenced phase observation must be modeled by Equation (18) in the navigation processor, which would clearly benefit from a stable user clock ($\Delta dt_{r;m,n} \approx 0$), in order to exploit the double-difference phase observation fully for user motion estimation.

Overall, we conclude that our first analysis of double-differenced phase observations indicates a number of pitfalls/points-of-further-investigation and they are less straight forward to use compared to single difference observations.

c) Insignificant Multipath

When computing Equation (9) and (10) we have assumed that the 'noise' can be modeled as additive white Gaussian even at single- and double-difference level. This is clearly true, if only the line-of-sight signal is present. In the case of (stronger) multipath products of line-of-sight and multipath components will emerge, which would require more detailed investigations, which are beyond the scope of this work.

Further discussions on difference correlators can be found in Chapter 10 of the book from Pany (2010).

5. Phase Locked-Loop with Difference Correlators

After the difference correlators have been formed with Equation (11), (12) or (16) they can be used for phase tracking. This tracking process is similar - but not identical - to conventional phase tracking. The difference is that no replica signal is generated and neither there is a correlation process. Instead the receiver maintains a carrier NCO whose phase value is denoted as $\hat{\phi}(t_u)$ where t_u is current epoch. The difference correlator (either single or double) value is denoted as $R(t_u)$. A phase discriminator $e_{PLL}(t_u)$ is formed by computing

$$e_{\text{PLL}}(t_u) = \arg\left\{R(t_u)e^{-j\hat{\phi}(t_u)}\right\}. \tag{21}$$

Here $\arg(x)$ is the phase between $\pm\pi$ of the complex number x. The remainder to the phase tracking loop, i.e. NCO update, loop filter, cycle slip detection, and so on remains the same as described e.g. by Morton (2021).

6. Motion Assisted Phase Unwrapping with Difference Correlators

Phase tracking for Starlink signals is clearly challenged by the short wavelength, making cycle-slips very likely to happen. Since our data sets can be post-processed, we tested another tracking method. First, we define a model for the line-of-sight dynamics $q_{\zeta(\mathbf{t})}$, which depends on the parameter vector ζ. For each processing epoch t_u we use the preceding N_u epoch to estimate the motion parameter by a least-squares fit to the complex phase of the difference correlator values as

$$\hat{\zeta}(t_u) = \arg\min_{\zeta} \sum_{v=u-N_u}^{u-1} \left(\arg\left\{R(t_u)e^{-jq_\zeta(t_v)}\right\}\right)^2. \tag{22}$$

The estimated $\hat{\phi}(t_u)$ phase at t_u is then given by the unwrapping process as

$$\hat{\phi}(t_u) = \arg R(t_u) + 2\pi\left[\frac{m_\zeta(t_u) - \arg R(t_u)}{2\pi}\right] \tag{23}$$

with $[x]$ being the nearest integer to the real number x (rounding operation). A characteristic of the phase values obtained via Equation (23) is that they are not impacted by any tracking loop dynamics.

V. EXPERIMENTAL SETUP: SIGNAL RECEPTION & MUSNAT SDR

In this section we first described the generic Starlink recordings setup for single antenna reception and then focus on the setup used to record signals from two antennas.

1. Single Antenna Recording

For the reception of the Starlink Ku-band downlink signal, the well-established signal reception setup at the Institute for Space Technology and Space Applications (ISTA) of the University of the Bundeswehr Munich is used (see Figure 5. This setup has been described in detail in multiple previous publications and is therefore only summarized here. Commercial off-the-shelf low noise blocks (LNBs) with a local oscillator (LO) frequency of 9.75 GHz are employed. The LNBs are powered via bias tees, which also allow the injection of an external reference signal (Lichtenberger et al., 2024, 2025).

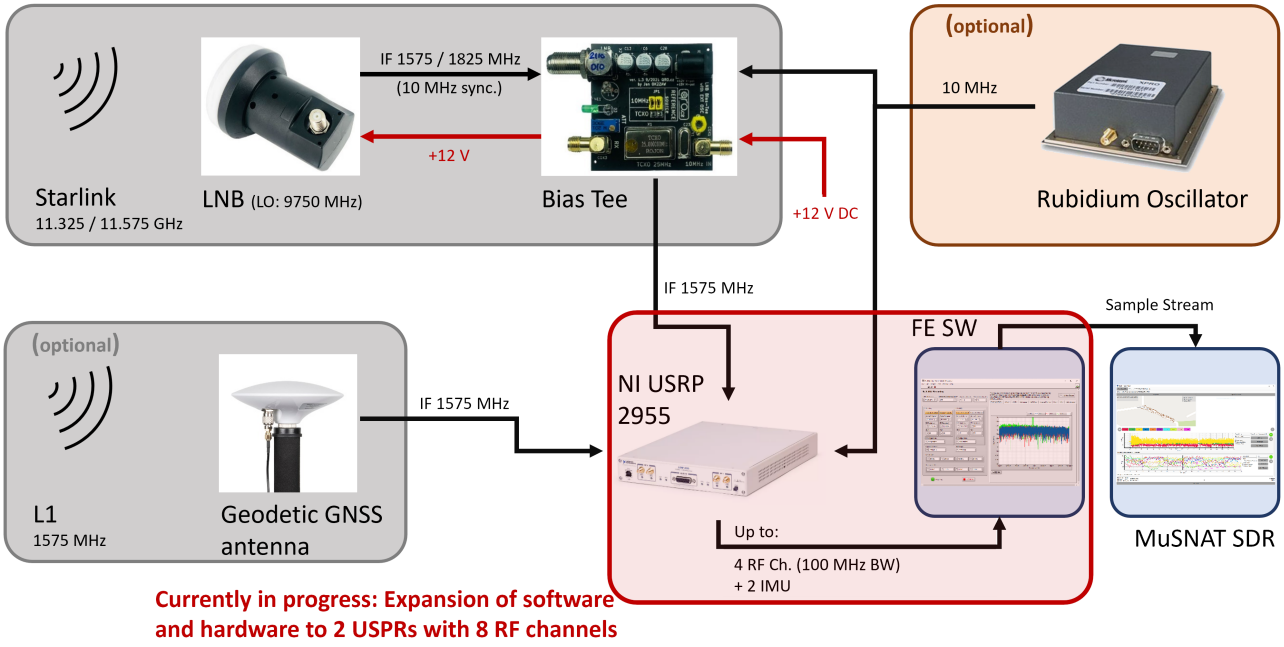


Figure 5: Flexible signal reception setup for Starlink Ku-band downlink signals

Optionally, a highly stable external 10 MHz reference (e.g., from a rubidium frequency standard) can be fed into the LNBs via the bias tee to mitigate the effects of the low-cost internal oscillators. For the experiments conducted here, the LNBs used were replaced with improved new versions. The new LNBs feature a more stable intermediate frequency (IF)/PLL integrated circuit (IC). The reason for the replacement was frequency offsets between synchronized LNBs of >100 Hz. These have now been eliminated. The LNBs are oriented towards the zenith and can be operated either with or without a parabolic dish, depending on the experiment configuration.

In addition to the Ku-band reception, an optional geodetic GNSS antenna is integrated into the setup to receive L1 signals. This enables the determination of a position, velocity and time (PVT) solution, which is used for reference timing and further analysis. The IF samples are digitized using a universal software radio peripheral (USRP)-based front-end and streamed to the receiver host system. In the current configuration, up to four radio frequency (RF) channels with bandwidths of up to 100 MHz can be recorded in parallel for a quantization of 2-bit I/Q. An extension of the setup to support eight RF channels using two synchronized USRPs is currently under implementation.

For the experiments presented in this paper, two Starlink channels (ch. 3: $f_{\mathrm{RF}} = 11{,}325.117188$ MHz and ch. 4: $f_{\mathrm{RF}} = 11{,}575.117188$ MHz) are recorded in parallel using a splitter connected to a each LNB. The signals are sampled with 4-bit quantization resolution at a rate of 50 MS/s per channel. Although the full Starlink channel bandwidth is 240 MHz, both the received signal and the replica are intentionally band-limited due to hardware limitations. In this work, a replica bandwidth of 42 MHz is used, resulting in a consistent band limitation on both sides of the correlation process.

Signal acquisition, tracking, and observable generation are performed using the Multi-Sensor Navigation Analysis Tool (MuSNAT) software-defined receiver. All GNSS receiver functions are implemented purely in software, providing high flexibility for algorithm development and rapid prototyping. MuSNAT supports all major GNSS constellations and frequency bands and can be extended with additional sensors such as inertial measurement units. For LEO SoOP, several dedicated extensions were implemented,

including the block-processing discriminator described in Section III.

The OFDM replica signals are generated using MATLAB and interfaced with the receiver through an existing software bridge. This approach allows rapid modification of the replica structure and enables the generation of both Starlink and simulated 5G NTN signals using a common processing framework. Furthermore, a satellite identification module based on estimated and predicted Doppler profiles assigns observations to individual transmitters. The resulting observables are stored in an adapted RINEX format tailored to LEO signals of opportunity and Starlink-specific channel characteristics.

2. Dual Antenna Recording

For the evaluation of the differential correlator-based tracking approach, a dedicated measurement configuration was employed using two independent Ku-band reception chains. Both chains observe the same Starlink downlink channels, ensuring identical signal content while enabling differential carrier phase analysis.

The differential measurement setup builds upon the previously described signal reception setup and employs two LNBs. One LNB is mounted statically and serves as a reference receiver. The second LNB is installed on a mechanically rotating platform to introduce a controlled and repeatable relative motion between the two reception points, thereby mimicking a dynamic user. The rotating LNB is positioned at a distance of approximately one meter from the static reference and follows a circular trajectory with a radius of about 50 cm. The rotation period is 2 s, corresponding to a rotation frequency of 0.5 Hz (see Figure 6.

Both LNBs are oriented towards the zenith and connected to the same receiver backend. The received signals are sampled synchronously and processed using identical tracking configurations. By maintaining the same Starlink channels and receiver parameters for both signal paths, external influences such as satellite motion, Doppler dynamics, and signal structure largely cancel out in the differential processing. The resulting carrier phase differences are therefore dominated by the controlled relative motion of the rotating platform and local receiver effects.

This measurement configuration enables a direct assessment of the differential correlator's ability to track relative carrier phase variations under realistic Starlink signal conditions, while providing a well-defined and repeatable carrier phase signature induced by the known circular motion.

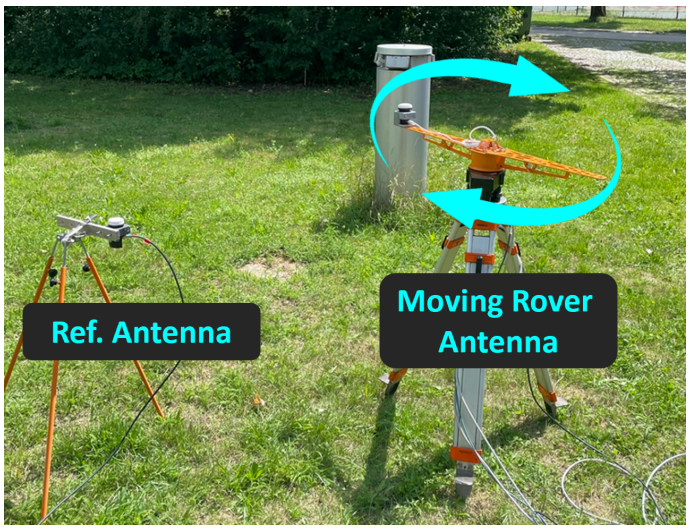


Figure 6: Setup used to record Starlink signals by two antennas. Left antenna: static reference station; right antenna: rover rotating with $r = 50$ cm and 30 rpm

VI. VALIDATION OF CARRIER PHASE TRACKING WITH SIMULATED SIGNAL

1. Simulation Scenarios and Filter Configurations

To validate the BPD and to assess the preservation of carrier phase information in both wide-range and narrow-range mode, simulation-based experiments were conducted using a synthetic 5G NTN signal with low medium earth orbit (MEO)-like orbital dynamics. The simulated dataset enables controlled evaluation of tracking behavior while retaining key characteristics such as OFDM modulation, sparse replica availability, and pronounced Doppler dynamics.

Two distinct filter configurations were investigated:

- **Filter mode 1 (unaided tracking):** A conventional tracking configuration employing a second-order DLL with a bandwidth

of 15 Hz, a second-order FLL with a bandwidth of 20 Hz, and a second-order PLL with a bandwidth of 20 Hz. All loops operate without mutual aiding.

- **Filter mode 2 (aided tracking):** A second-order FLL-aided third-order PLL combined with a first-order carrier aided DLL. The loop bandwidths are identical to those used in filter mode 1.

This separation allows the influence of loop aiding on stability, convergence, and phase preservation to be analyzed independently of the block-processing mechanism itself. For both filter configurations, the PLL was activated with a delay of 5 s after tracking start to ensure initial frequency convergence of the FLL before carrier phase tracking.

2. Forced Wide-Range / Narrow-Range Mode Switching

To explicitly verify that carrier phase information is preserved not only in narrow-range but also during wide-range block-processing operation, the tracking mode was deliberately controlled over the duration of the simulation. For the first 60 s, the wide-range mode was enforced. This was followed by 60 s of narrow-range tracking, after which the wide-range mode was re-enabled and maintained until the end of the dataset.

This artificial mode switching allows direct observation of potential discontinuities, bias changes, or loss of phase coherence when transitioning between tracking modes. Any degradation of carrier phase observables caused by the wide-range block-processing operation would therefore become immediately visible in the tracking logs.

3. Evaluated Tracking Metrics

For both filter configurations, the following quantities were extracted from the MuSNAT tracking logs and visualized using MATLAB:

- DLL discriminator error (in subchips)
- FLL discriminator error (in Hz)
- PLL discriminator error (in cycles)
- Estimated Doppler frequency (in Hz)
- Estimated code rate (in subchips/s)
- Code-minus-carrier (CMC) observable (in meters)
- Prompt correlator magnitude (unitless)
- Estimated signal strength (carrier-to-noise-density ratio (C/N_0), in dB-Hz)

These metrics jointly provide insight into tracking loop stability, convergence behavior, noise characteristics, and the consistency between code and carrier tracking.

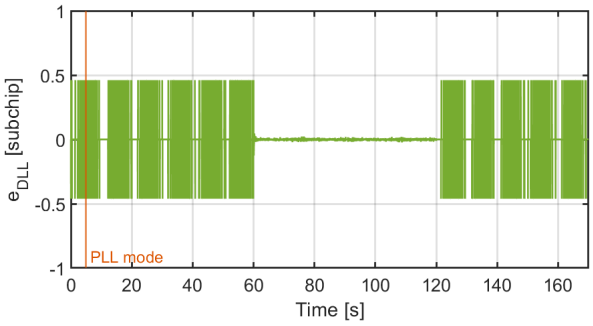
4. Simulation Results: Filter mode 1

Figure 7 shows the tracking results obtained using filter mode 1 (unaided tracking). The enforced wide-range and narrow-range tracking intervals are clearly visible across all subplots. In wide-range mode, the code phase discriminator output (Figure 7a) exhibits distinct jumps between two values (approximately -0.5 m and $+0.5$ m, corresponding to a subchip length of 3.253 m). This behavior results from the maximum detected in wide-range mode alternating between two adjacent multi-correlator positions. A similar effect is observed in the frequency discriminator, where the estimated frequency alternates between approximately -2.5 Hz and $+2.5$ Hz (Figure 7b). This behavior is attributable to the discrete resolution of the frequency-domain search grid.

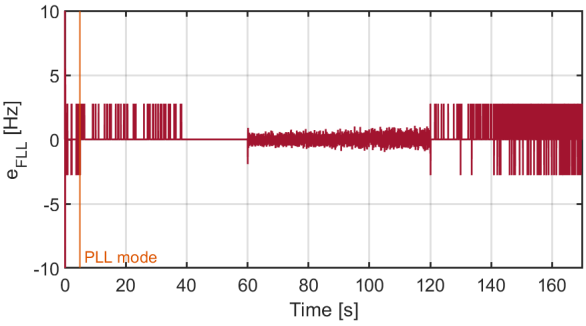
The observed jumping behavior could be reduced by increasing the resolution in both the code phase (multi-correlator) and frequency dimensions. At the same time, the overall multi-correlator search range could be reduced, which would likely result in a more consistent number of samples contributing to the estimation process. In contrast, narrow-range mode exhibits very stable tracking behavior, with only small discriminator errors.

The activation of the PLL at $t = 5$ s is clearly visible in the carrier phase discriminator plot (Figure 7c). While wide-range mode has only a minor impact on PLL performance in this configuration, narrow-range mode shows slightly increased noise, although tracking remains stable. The residual oscillatory behavior may indicate a marginally suboptimal loop bandwidth setting. This hypothesis is supported by the visible offset of the carrier phase discriminator error.

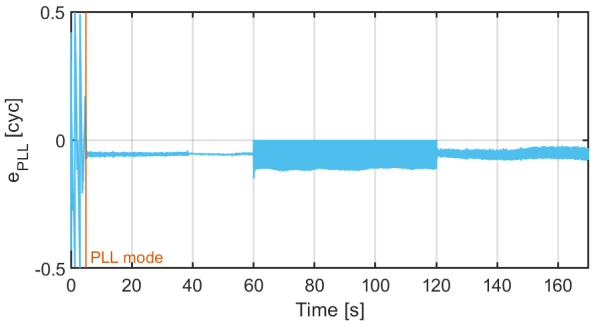
The estimated Doppler frequency evolves smoothly over time (Figure 7d). The alternating behavior between adjacent multi-correlator positions is also reflected in the estimated code-rate during wide-range operation (Figure 7e). In narrow-range mode, however, the code-rate estimate exhibits low noise. This behavior is consistently reflected in the CMC observable (Figure 7f). In wide-range mode, deviations of up to approximately ± 1 m are observed, whereas in narrow-range mode the CMC remains within the centimeter range.



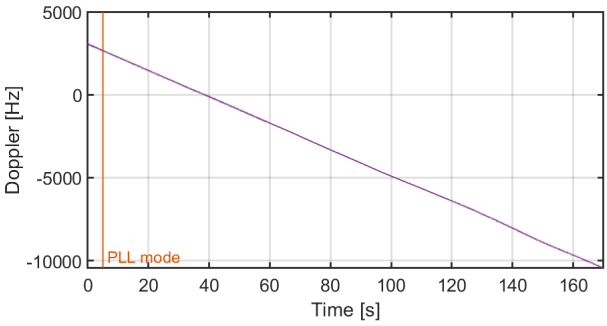
(a) DLL discriminator values



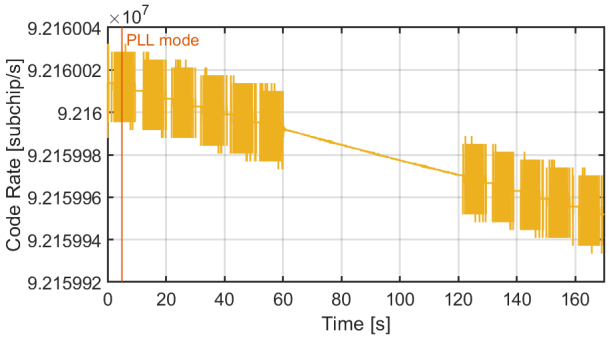
(b) FLL discriminator values



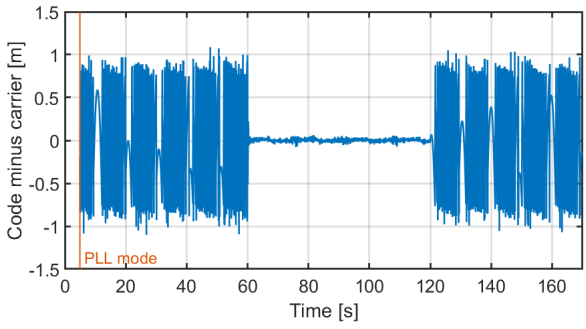
(c) PLL discriminator values



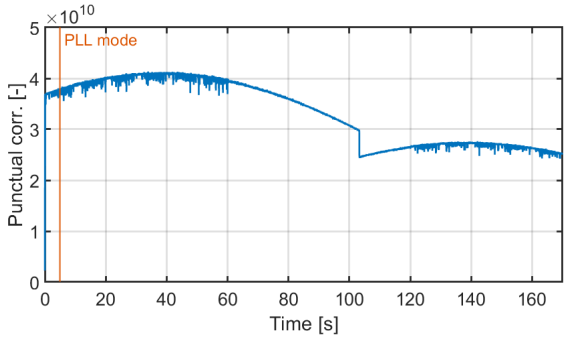
(d) Estimated Doppler



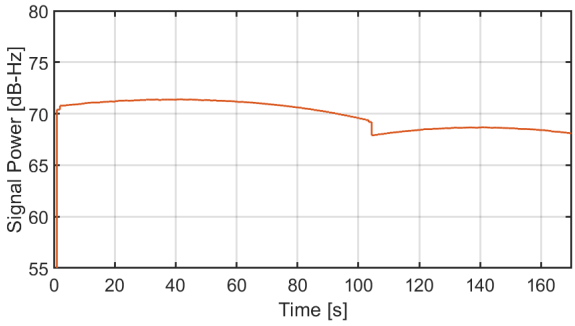
(e) Estimated Code rate



(f) CMC values



(g) Prompt correlator values



(h) Received C/N_0

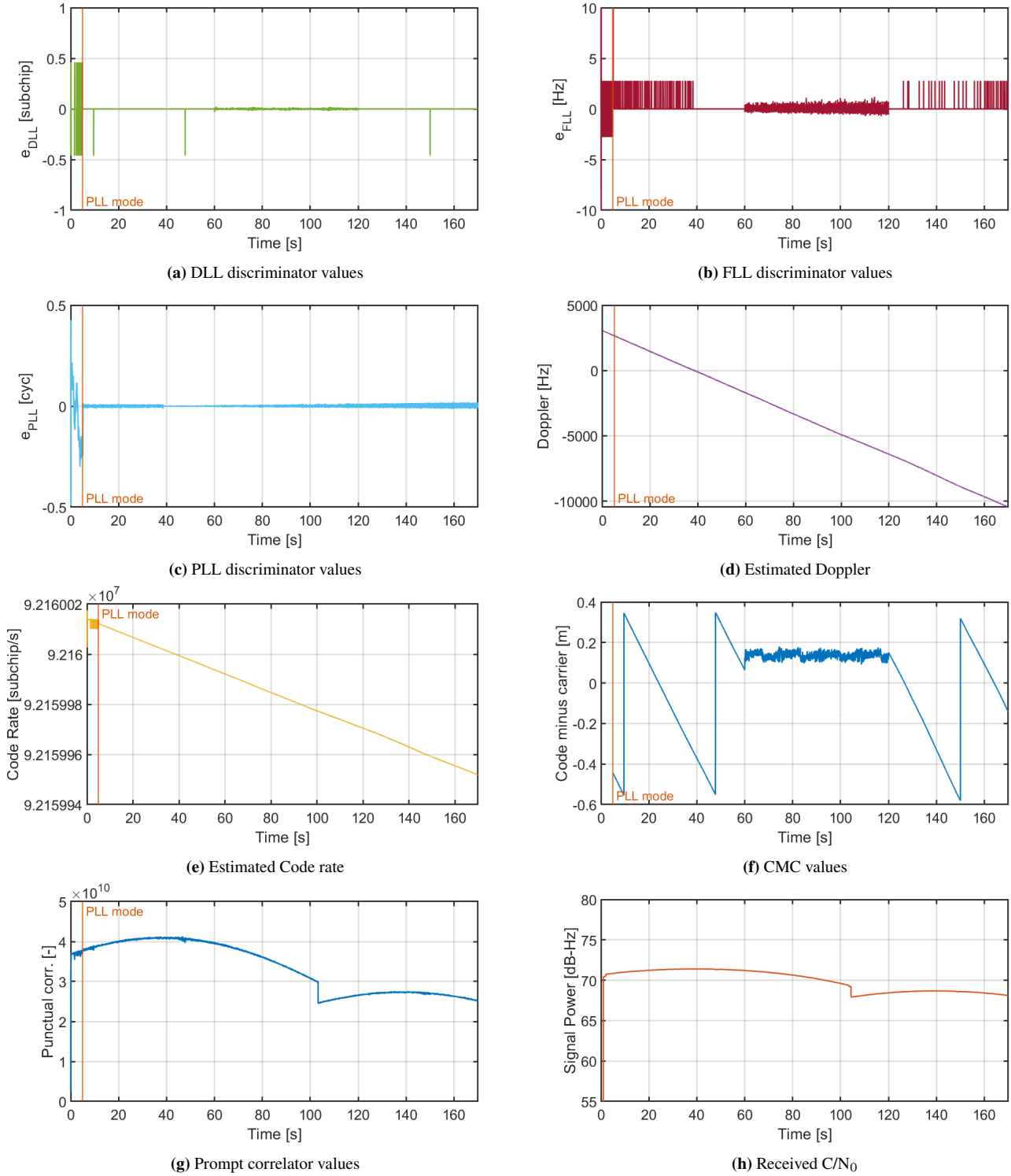
Figure 7: Visualization of tracking results for simulated 5G NTN signals with standard tracking loops

The prompt correlator magnitude further illustrates the difference between the two modes (Figure 7g). In wide-range mode, the signal is not detected consistently perfectly in every epoch, whereas narrow-range mode shows a clean and highly stable prompt correlator response with very low noise. The corresponding simulated signal strength is shown in Figure 7h.

Importantly, no carrier phase discontinuities or loss of phase coherence are observed when transitioning between wide-range and narrow-range tracking. This confirms that the block-processing discriminator preserves carrier phase information across both

operating modes, despite the discrete nature of the wide-range search.

5. Simulation Results: Filter mode 2



(a) DLL discriminator values

(b) FLL discriminator values

(c) PLL discriminator values

(d) Estimated Doppler

(e) Estimated Code rate

(f) CMC values

(g) Prompt correlator values

(h) Received C/N_0

Figure 8: Visualization of tracking results for simulated 5G NTN signals with FLL aided PLL and PLL aided DLL

In filter mode 2 (see Figure 8), the jumping between multi-correlator positions observed in wide-range mode for filter mode 1 is largely eliminated. Only three isolated outliers are visible in the code phase discriminator at approximately 10 s, 48 s, and

150 s. In all other epochs, the tracking remains at the correct multi-correlator position, as indicated by a DLL error of zero. In narrow-range mode, the code phase error exhibits extremely low noise, remaining in the centimeter range (Figure 8a).

As in filter mode 1, discrete jumps are still present in the frequency discriminator during wide-range operation, reflecting the finite resolution of the frequency-domain search (Figure 8b). However, due to the improved alignment between code, frequency, and carrier tracking, the carrier phase discriminator error is now extremely low throughout the dataset once the PLL is activated at $t = 5$ s (Figure 8c). No noticeable discontinuities are observed when transitioning between wide-range and narrow-range modes, indicating consistent phase behavior across both tracking regimes.

The estimated Doppler frequency evolves smoothly over time, with no observable degradation during wide-range operation (Figure 8d). The same applies to the estimated code-rate, which follows a smooth and well-defined trajectory once the PLL has been activated (Figure 8e). The three isolated outliers observed in the code phase discriminator are also visible in the CMC observable, where they manifest as short sawtooth-like deviations in wide-range mode due to slight overshoot behavior (Figure 8f). Overall, the CMC remains within approximately $[-0.6,\ 0.4]$ m during wide-range operation and within a few centimeters in narrow-range mode.

Finally, the prompt correlator magnitude exhibits a consistent and stable behavior across both tracking modes, indicating reliable signal detection throughout the entire simulation (Figure 8g + (Figure 8h)).

6. Discriminator Statistics

The quantitative impact of loop aiding is summarized in Table 1, which lists the variances of the DLL, FLL, and PLL discriminator outputs for both filter configurations over the entire processing period. Compared to filter mode 1, filter mode 2 exhibits a substantial reduction in discriminator variance across all tracking loops. In particular, the DLL variance is reduced by approximately one order of magnitude, decreasing from 0.2063 m to 0.0203 m. A similar improvement is observed for the PLL, where the carrier phase variance decreases from 0.0462 cycles to 0.0030 cycles, indicating significantly improved carrier phase stability.

Table 1: Comparison of achieved discriminator variances for filter mode 1 and filter mode 2

	σ_{DLL}	σ_{FLL}	σ_{PLL}
Filter mode 1	0.2063 m	0.2176 Hz	0.0462 cyc
Filter mode 2	0.0203 m	0.1717 Hz	0.0030 cyc

The FLL variance is also reduced when using aided tracking, decreasing from 0.2176 Hz to 0.171 Hz. While this improvement is less pronounced than for the DLL and PLL, it confirms that loop aiding primarily benefits code and carrier phase consistency, while frequency tracking is already sufficiently stable in the unaided configuration.

These results quantitatively confirm the observations from the time-domain plots and demonstrate that filter mode 2 provides a clear performance advantage under controlled simulation conditions, particularly with respect to carrier phase stability.

7. Discussion of Simulation Results

The simulation results confirm that the block-processing discriminator preserves carrier phase information in both wide-range and narrow-range operation modes. While the unaided configuration demonstrates correct tracking behavior under controlled conditions, aided tracking significantly improves robustness and noise performance.

These findings validate the block-processing framework and motivate its application to real Starlink measurements, where signal sparsity and carrier phase instability are more pronounced.

VII. REAL WORLD CARRIER PHASE TRACKING PERFORMANCE

1. PLL and BPD Tracking with a Single Antenna

a) Measurement Configuration

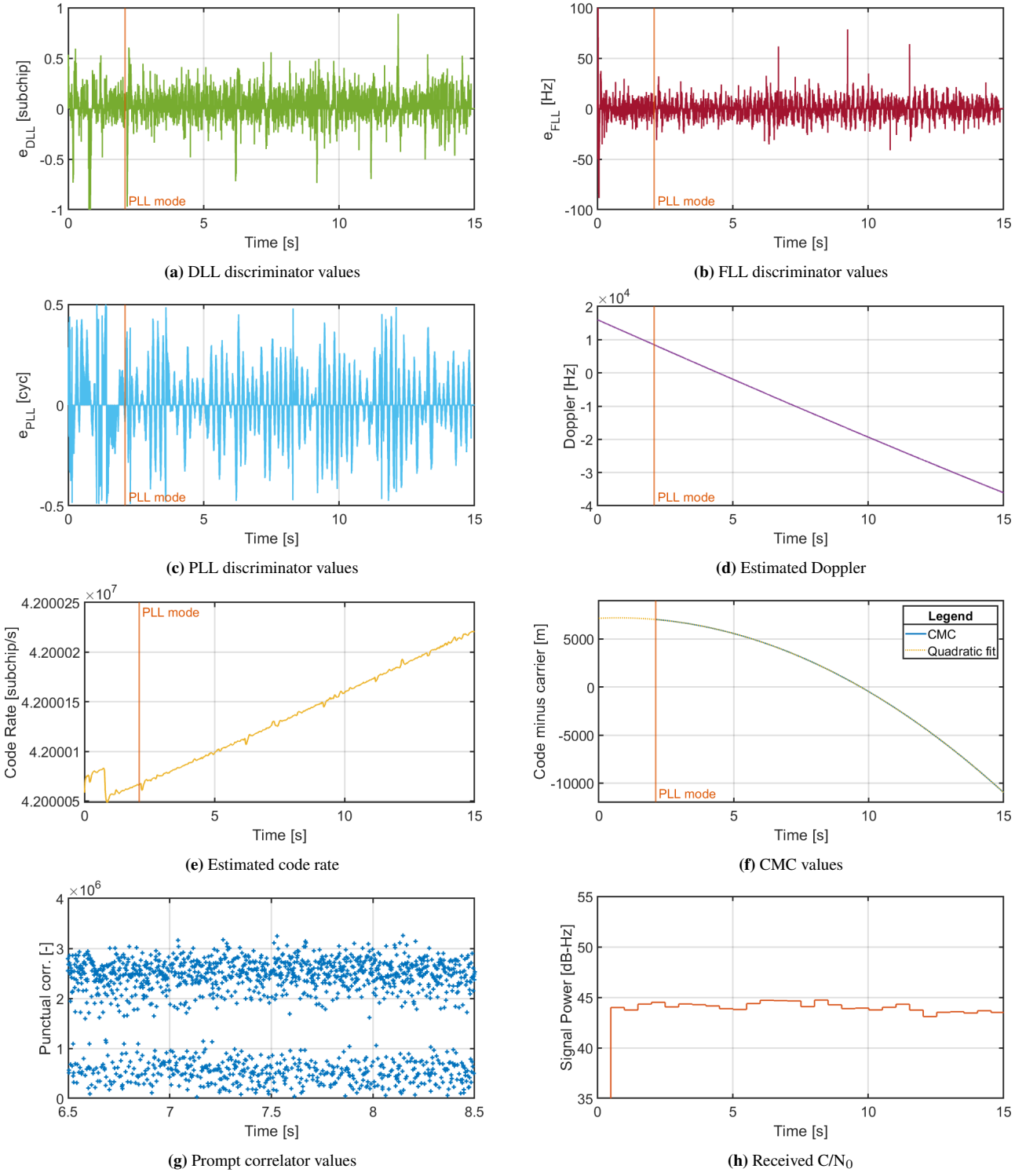
The following results were obtained from a real Starlink Ku-band downlink measurement using the block-processing-based tracking approach described in Section III. The measurement was performed on September 25, 2025 (6:30:46 global positioning system (GPS) time) using two antennas simultaneously: one statically mounted antenna and one antenna mounted on a rotating platform. Both antennas observed the same Starlink channels and satellites at the same time and were processed using identical receiver and tracking configurations.

For all results presented in this section, filter mode 2 was applied, employing an FLL-aided third-order PLL without DLL aiding. DLL aiding was omitted, as code–carrier divergence was observed for Starlink signals. The block-processing discriminator was

used to generate RINEX observables for both antennas independently.

b) Undifferenced Tracking Results

Figure 9 shows the undifferenced tracking results obtained for the static antenna using the block-processing-based approach with filter mode 2 over a complete FAI of approximately 15 s. The PLL was activated after 2 s to allow initial frequency convergence. Note that the PLL activation delay differs between simulation and real measurements due to different convergence requirements.



(a) DLL discriminator values

(b) FLL discriminator values

(c) PLL discriminator values

(d) Estimated Doppler

(e) Estimated code rate

(f) CMC values

(g) Prompt correlator values

(h) Received C/N_0

Figure 9: Visualization of tracking results for static LNB receiving Starlink ch. 3

Over the entire observation interval, the code phase discriminator error exhibits noise on the order of ± 0.5 m, with several isolated outliers (Figure 9a). A similar behavior is observed for the frequency discriminator error, which remains within approximately ± 25 Hz, with distinct outliers occurring at approximately 7 s, 9 s, and 11.5 s (Figure 9b). These outliers coincide with transient disturbances in the tracking process and are consistently reflected across multiple observables.

After PLL activation, the carrier phase discriminator error exhibits oscillatory behavior with varying amplitude, indicating that the PLL is unable to fully follow the rapid carrier phase dynamics inherent to the Starlink signal (Figure 9c). Nevertheless, continuous carrier phase tracking is maintained throughout the measurement interval. Only three clear cycle slips are observed at approximately 8 s, 11.5 s, and 12 s, demonstrating that phase lock is largely preserved despite the challenging signal conditions.

The outliers observed in the code phase discriminator error are also clearly visible in the estimated code rate (Figure 9e). Aside from these isolated events, the code-rate estimate remains highly stable after approximately 1 s. The estimated Doppler frequency evolves smoothly over time, with no observable degradation (Figure 9d). The divergence between code and carrier tracking is clearly reflected in the CMC observable (Figure 9f). A quadratic fit to the CMC reveals an almost perfectly quadratic behavior, given by

$$\mathrm{CMC}(t) = -89.09\ \mathrm{m/s^2} \cdot t^2 + 128.4\ \mathrm{m/s} \cdot t + 7140\ \mathrm{m},$$

indicating systematic and time-correlated inconsistencies between code and carrier phase tracking rather than random noise.

The prompt correlator magnitude plot shows a zoomed view of a 2 s interval (Figure 9g). During this interval, it is evident that the correlation peak is not consistently hit perfectly, reflecting the sparse replica structure and residual tracking errors. Despite this, the estimated signal strength remains relatively stable over the entire FAI, ranging between approximately 43 and 45 dB-Hz, with no indication of sustained signal loss (Figure 9h).

Overall, the static antenna results demonstrate that, while undifferenced carrier phase tracking of real Starlink signals remains inherently unstable, the block-processing-based approach enables continuous carrier phase tracking with bounded errors. The extracted carrier phase observables retain sufficient coherence to support subsequent differential processing, as demonstrated in the following section.

Figure 10 shows the undifferenced tracking results obtained for the rotating antenna using the same block-processing-based configuration and filter mode 2. Overall, the tracking behavior is qualitatively very similar to that observed for the static antenna. The discriminator errors (Figure 10a - 10c), estimated Doppler frequency, code rate, and CMC observable exhibit comparable characteristics (Figure 10d - 10f), including bounded errors, isolated outliers, and residual divergence between code and carrier tracking given by

$$\mathrm{CMC}(t) = -89.1\ \mathrm{m/s^2} \cdot t^2 + 29.29\ \mathrm{m/s} \cdot t + 8015\ \mathrm{m}.$$

A key difference becomes apparent in the prompt correlator magnitude (Figure 10g). In contrast to the static case, the prompt correlator exhibits a clear sinusoidal modulation. This behavior is most evident in the zoomed 2 s interval and directly reflects the periodic relative motion introduced by the rotating antenna platform. The sinusoidal variation indicates that the correlation peak is periodically approached and receded as a function of the antenna motion.

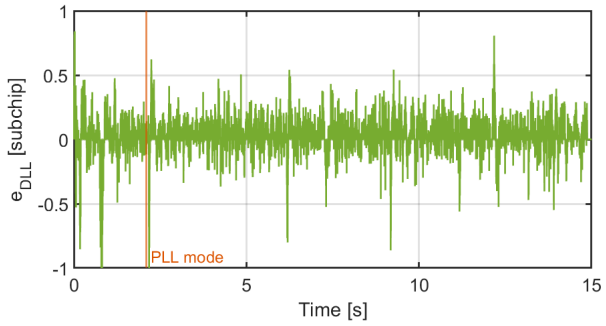
A corresponding periodic behavior is also visible in the estimated signal strength (Figure 10h). The received C/N_0 oscillates between approximately 43 and 45 dB-Hz, in clear contrast to the more stationary behavior observed for the static antenna. This modulation is consistent with the changing relative geometry and coupling conditions induced by the rotation.

Apart from these motion-induced effects in the prompt correlator magnitude and signal strength, no additional degradation of the undifferenced tracking performance is observed. The similarity between the static and rotating antenna results confirms that the block-processing-based approach captures the dominant signal dynamics consistently for both measurement configurations, while the rotation-induced effects are primarily manifested in amplitude-related observables rather than in the carrier phase estimates themselves.

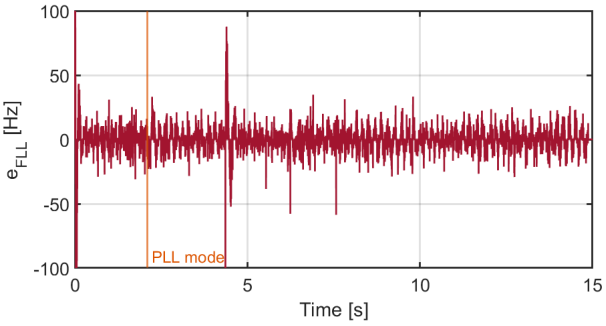
Table 2: Comparison of achieved discriminator variances for static and rotating antenna

	σ_{DLL}	σ_{FLL}	σ_{PLL}
static antenna	0.5366 m	4.6949 Hz	0.0793 cyc
rotating antenna	0.5318 m	7.0346 Hz	0.0749 cyc

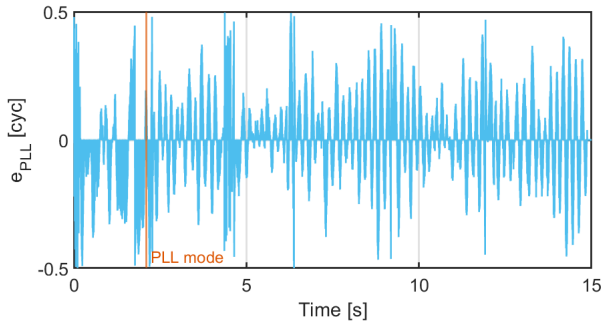
Table 2 summarizes the variances of the DLL, FLL, and PLL discriminator outputs for the static and rotating antenna configurations. The results show that the discriminator variances are of comparable magnitude for both antennas. The DLL variance



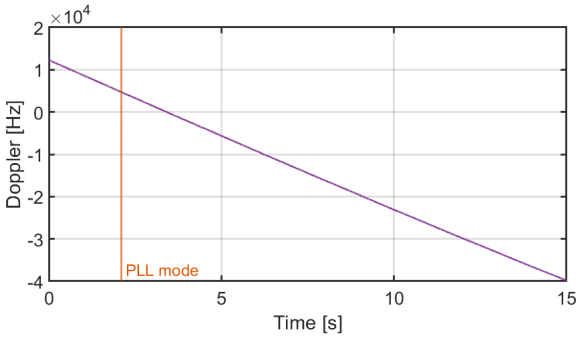
(a) DLL discriminator values



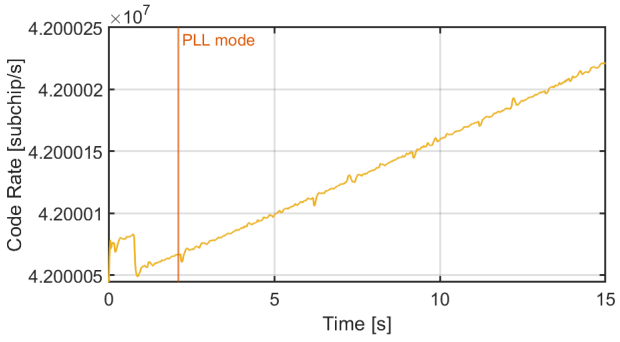
(b) FLL discriminator values



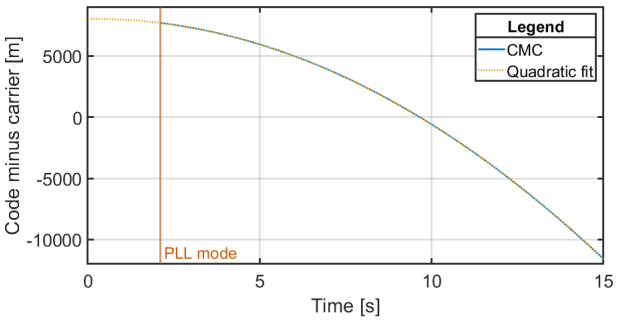
(c) PLL discriminator values



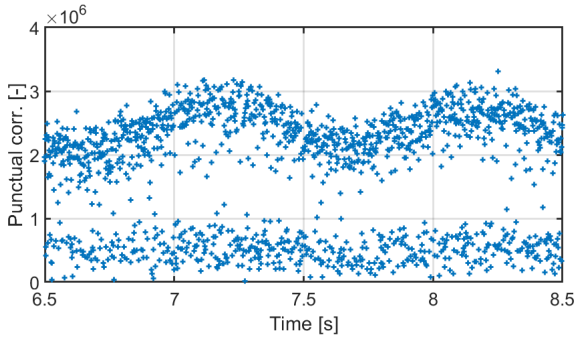
(d) Estimated Doppler



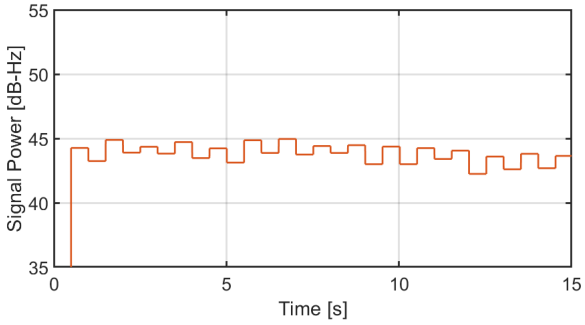
(e) Estimated code rate



(f) CMC values



(g) Prompt correlator values



(h) Received C/N_0

Figure 10: Visualization of tracking results for rotating LNB receiving Starlink ch. 3

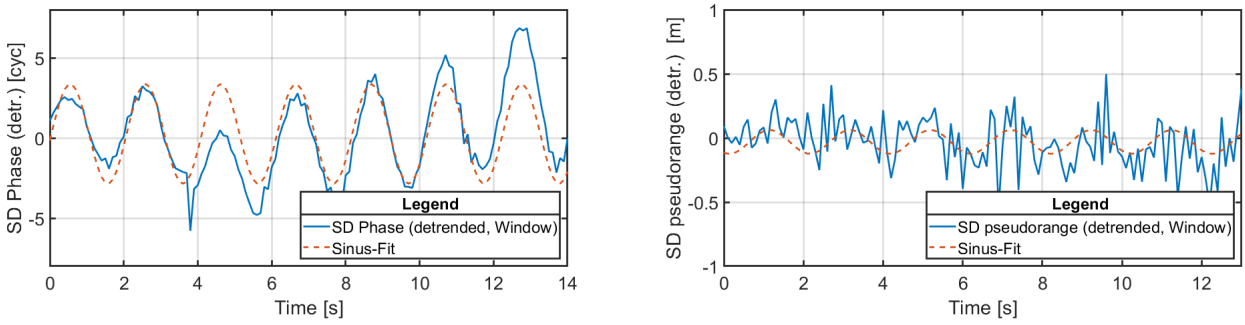
remains nearly identical, with values of 0.5366 m for the static antenna and 0.5318 m for the rotating antenna, indicating similar code tracking behavior in both configurations.

The PLL discriminator variance is likewise comparable, with values of 0.0793 cycles and 0.0749 cycles for the static and rotating antennas, respectively. This confirms that the overall carrier phase stability achieved with the block-processing-based approach is not significantly degraded by the additional motion introduced by the rotating platform.

A moderate increase in FLL variance is observed for the rotating antenna, increasing from 4.6949 Hz to 7.0346 Hz. This increase is consistent with the additional dynamics introduced by the controlled antenna motion and reflects the increased frequency variability observed in the undifferenced measurements. Overall, the results indicate that the dominant limitations in undifferenced Starlink carrier phase tracking are not driven by local antenna motion but by common-mode effects inherent to the non-cooperative signal itself.

c) Single-Difference Analysis Based on BPD Observables

To further assess the carrier phase stability achieved with the block-processing-based approach, the carrier phase and pseudorange observables generated by MuSNAT were exported in RINEX format and processed offline. Single differences were formed between the static and rotating antenna observations for identical satellites (one Starlink space vehicle (SV) at ch. 3) and epochs. Since both antennas were measured simultaneously, common-mode effects such as satellite-induced Doppler dynamics and transmitter-related phase variations largely cancel out in the single-difference observables.



(a) Carrier phase single difference

(b) Pseudorange single difference

Figure 11: Visualization of single differences between static and rotating LNB

Figure 11 shows the single differences of the carrier phase and the pseudorange, plotted side by side. For the carrier phase, a linear trend was removed to isolate the relative motion-induced component. A sinusoidal model was subsequently fitted to the detrended carrier phase observation. The resulting carrier phase single difference follows the fitted sinusoid very closely, indicating a clear and consistent periodic behavior. The estimated frequency of the sinusoid is approximately 0.5 Hz, which matches the known rotation frequency of the antenna platform. The observed amplitude spans several carrier phase cycles, demonstrating the high sensitivity of the carrier phase observable to the relative antenna motion.

The single difference of the pseudorange was processed analogously by removing a linear trend and applying a sinusoidal fit. Due to the significantly higher noise level of the pseudorange observable, the sinusoidal variation is less clearly visible in the time domain. Nevertheless, the fitted sinusoid again yields a frequency that closely matches the true rotation frequency of the platform. The estimated amplitude lies in the decimeter range, which is consistent with the physical radius of the rotating antenna ($r \approx 50$ cm). It should be noted that the observed amplitude corresponds to the projected radius along the line of sight to the satellite. A precise quantitative interpretation would therefore require correction for the instantaneous satellite geometry and orbit.

d) Discussion

The real-measurement results show that undifferenced carrier phase tracking of Starlink signals using block-processing remains challenging due to signal sparsity and inherent phase instability. However, the simultaneous dual-antenna measurement demonstrates that the block-processing-based approach yields carrier phase observables of sufficient quality to support single-difference processing.

The clear visibility of the rotation-induced carrier phase signature in the single-difference observables confirms that the block-processing discriminator preserves carrier phase information to a degree that enables differential applications. This finding bridges the gap between the undifferenced block-processing results and the fully differential correlator-based approach presented in the following section.

2. Use of Difference Correlators

We conducted approximately 30 measurements in summer 2025 using the dual-antenna setup shown in Figure 6. Selected results are discussed in this section. A receiver configuration with two RF channels connected to each LNB was used. One channel was configured to receive Starlink channel no. 3 ($f_{\mathrm{RF}} = 11{,}325.117188$ MHz), and the other to receive Starlink channel no. 4 ($f_{\mathrm{RF}} = 11{,}575.117188$ MHz). in-phase and quadrature (I/Q) sampling at 50 MHz with 4-bit quantization was employed.

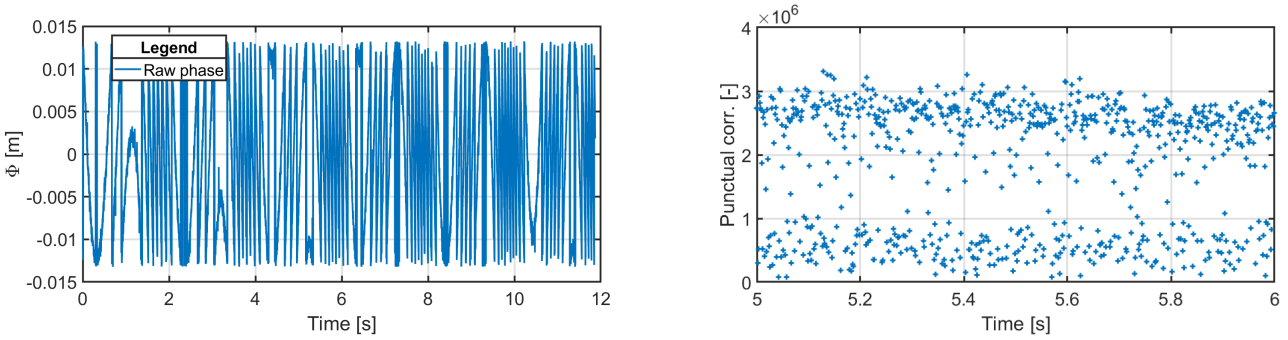


Figure 12: Left: phase of single-differenced correlator values (rotating antenna, clocks synced, ch. 3), right: magnitude of reference station prompt correlator

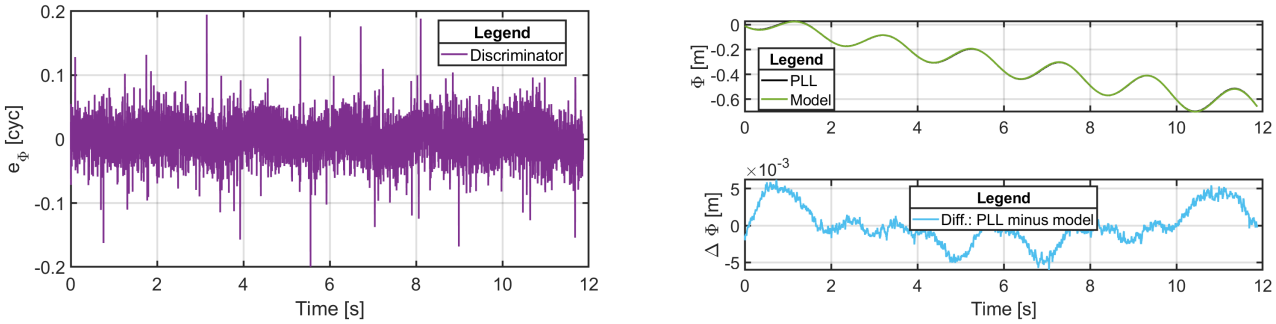


Figure 13: PLL tracking of the data from Figure 12 with B_{PLL}=35 Hz; left: phase discriminator, right: resulting phase and best fit for comparison

The signals were acquired on the reference-station antenna with a coherent integration time of 1.3333 ms and 16 non-coherent integrations. The tracking channels of the rotating rover antenna were slaved to the corresponding reference antenna channels (i.e., they shared the same NCO). Tests with independent channels were also conducted to verify that the computation of Equations (7) and (11) is independent of the tracking mode. Slaving was ultimately chosen, as it ensured more homogeneous data availability.

Each recording lasted approximately 5 minutes and typically contained several Starlink broadcasts. In many cases, transmissions were present during only a single FAI (15 s); in rare cases, they covered multiple intervals. Channels 3 and 4 exhibited similar transmission probabilities; simultaneous transmission on both channels was observed only in a few selected cases. For the analysis, we focus exclusively on strong-signal recordings originating from the main satellite lobe. We did not have the capability to identify the transmitting satellite identifiers (IDs); however, this information is not required for our purposes, as the satellite position is irrelevant.

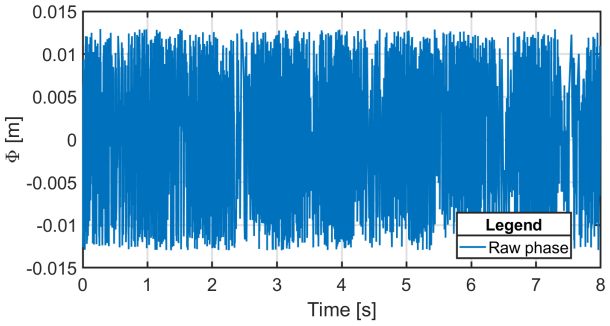
a) Single Difference

Figure 12 shows the carrier phase of the single difference prompt correlator values as computed by Equation (11). The recording was done on Starlink channel 3. The signal showed a good frame occupancy (2/3 of the frames occupied). A threshold of 7×10^5 for reference/rover prompt correlator values, shown on the right side of Figure 12, was chosen to qualify them as signal and only those values are used for the subsequent processing steps. The phase values shown on the left side of Figure 12 indicate already smooth behavior.

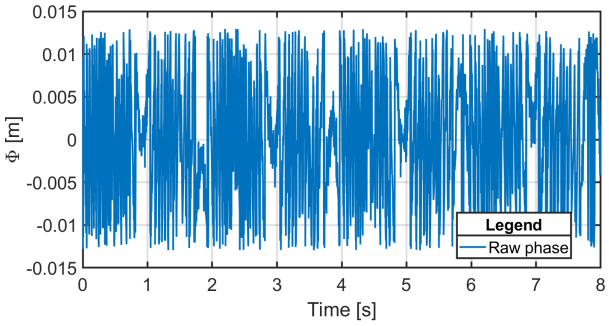
Indeed when applying a 2nd order PLL with a bandwidth of 35 Hz as described in Section IV.5, the discriminator values computed via Equation (21) and shown in Figure 13 indicate stable phase tracking. The resulting estimated phase is shown on the upper right plot of Figure 13 as the black curve. Since no ground truth was available, a motion model was fitted to the phase data. It models the motion as sinusoidal variation with linearly changing amplitude plus a linear trend. The residuals to this model are shown in the lower left plot and confirm that the estimate is smooth and that it does not contain any cycle slip.

We conclude that the recording of Figure 12 has a decent quality. Since reference station and rover signals were captured by the same USRP, which also delivered a 10 MHz signal to the LNBs, the receiver clock difference $dt_{r;m,n}$ basically vanishes. The phase data can be used to estimate to motion of the rover following the model of Equation (9). Many other recordings of similar good quality have been found, especially when using the new LNBs.

During our first measurements with the dual antenna setup, we observed recordings of purer quality when using the old LNBs.

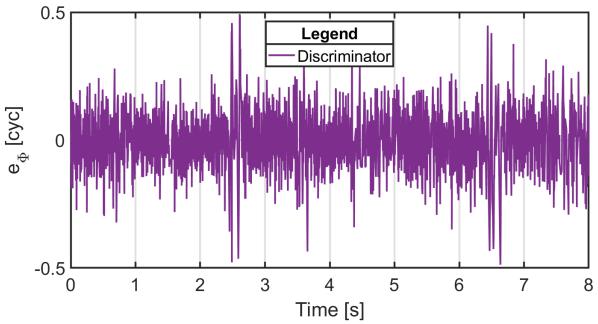


(a) Phase of single-differenced correlator values (rotating antenna, clocks not synced, ch. 4)



(b) Phase of double-differenced correlator values (rotating antenna, clocks not synced, ch. 3+4)

Figure 14: Comparison of the phase from single-differenced and double-differenced correlator values



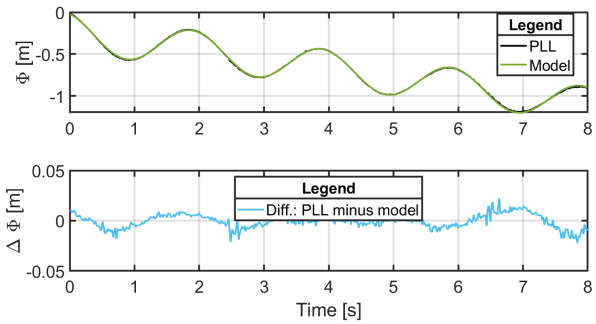


Figure 15: PLL tracking of the data from Figure 14b with B_{PLL}=35 Hz; left: phase discriminator, right: resulting phase and best fit for comparison

One example is shown in Figure 14a. Reference and rover signal have still been captured by the same USRP, but we suspect that the sync of the LNBs to the USRP was not working correctly. As a consequence, the phase of the single difference correlator is basically noise-like. A number of attempts with various PLL parameters and the motion assisted unwrapping have been used to track this signal, but they all turned out to produce only meaningless data and are thus now shown here. Only double-differencing removed the LNB impact and is discussed in the following.

b) Double Difference

For the data set of Figure 14a also Starlink signals on channel 3 have been detected. It was thus possible to form double-differenced correlator values according to Equation (12). An amplitude threshold for both channels and both receiver was applied to qualify prompt correlator values for the processing. The resulting double-differenced phase is shown in Figure 14b and could be successfully tracked with 2nd order PLL of 35 Hz bandwidth (cf. Figure 15). In Section IV.4 b) we showed that double differencing actually not fully eliminates the receiver clock error (the LNB jitter is considered to be part of this) but only reduces its impact by a factor of 11.4 GHz/250 MHz $\approx$ 46. This was obviously sufficient to allow phase tracking.

To underline the tight limits in phase tracking, Figure 16 shows tracking results for the same data set but with a slightly different bandwidth of 30 Hz. At around $t = 6.6$ s the PLL gets unstable and a cycle slip occurs. It last until $t = 6.9$ s and afterwards the PLL returns to stable tracking again.

The alternate tracking method described in Section IV.6 has also been tested with double-difference data. The four elements of the motion model parameters ζ are: amplitude and phase of a sinusoidal variation with a period of 2.01 s, a constant offset and a linear trend. The last $N_u = 100$ correlator points are considered in each fit (one fit is shown on the left side of Figure 17). The resulting phase estimate shown on the right side of Figure 17 appears to be more noisy than its counterpart of Figure 15, which is expected as this unwrapping procedure does not contain any filtering.

c) Summary of Single/Double Difference Tracking

Overall we conclude that phase tracking of single and double difference correlator values is clearly possible. The short wavelength and the intermittent nature of the Starlink broadcasts results in a very low margin making cycle-slips likely. Two tracking methods, PLL and motion assisted unwrapping, have been tested but further research is needed to better understand which of them fits better to the various applications. In Section IV we concluded that single-difference phase values are most likely better suited for

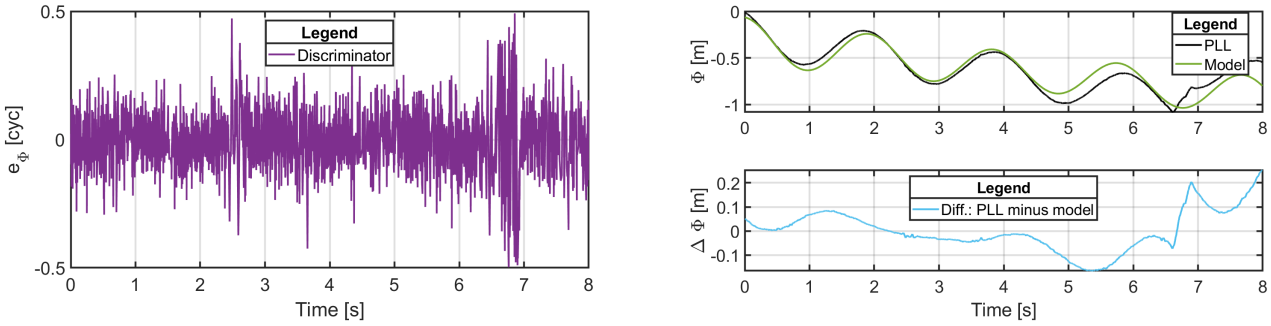


Figure 16: PLL tracking of the data from Figure 14b with B_{PLL}=30 Hz; left: phase discriminator, right: resulting phase and best fit for comparison

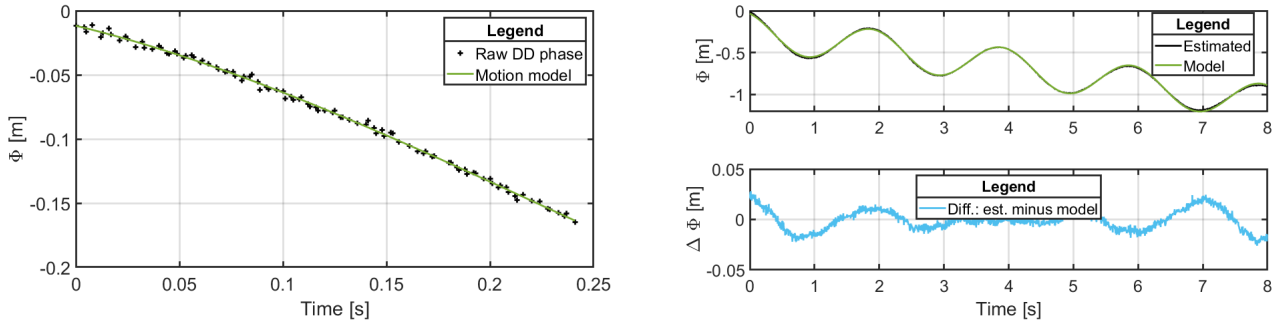


Figure 17: Motion assisted unwrapping of the data from Figure 14b; left: single iteration, right: right: resulting phase and best fit for comparison

navigation purposes as double-differenced phase values require some approximations due to the different carrier frequencies. It should be noted, that our experiments captured both signals by the same frontend but in upcoming studies we will use different frontends to better understand the impact of the receiver oscillator jitter on phase tracking (we expect that a high quality oscillator might be needed to allow phase recovery).

VIII. CONCLUSION

This paper investigated carrier phase tracking of sparse LEO signals of opportunity, with a particular focus on the Starlink Ku-band downlink. Due to the non-cooperative nature of such signals, only a small fraction of the transmitted waveform is known and repeatable, which severely limits the usable correlation energy and challenges conventional tracking loop designs.

Two complementary carrier phase tracking approaches were investigated. First, a block-processing-based tracking method employing a block-processing discriminator was implemented and extended with a carrier phase discriminator within the MuSNAT software-defined receiver. The approach was evaluated using real-time Starlink measurements. The results demonstrate that meaningful carrier phase observables can be obtained using only PSS/SSS-based replicas with limited bandwidth, despite the highly sparse signal structure and pronounced LEO-induced Doppler dynamics.

Second, a differential correlator-based tracking approach was evaluated using a dedicated dual-receiver measurement setup. The experimental results confirm that carrier phase tracking of Starlink signals is also feasible using differential processing, enabling reliable observation of relative carrier phase variations under controlled dynamic conditions. This approach provides a complementary perspective and is particularly well suited for relative navigation or attitude-related applications.

The presented results rely exclusively on PSS/SSS-based replicas and do not require access to the full Starlink beacon or obsolete tone-based tracking. While this represents a conservative use of the available signal structure, it demonstrates the robustness of the proposed methods under restrictive conditions. A direct comparison of phase-locked loop performance using PSS/SSS-only replicas versus full-beacon-based replicas remains an important topic for future work.

Beyond carrier phase tracking itself, the ability to extract stable carrier phase observables from sparse LEO signals opens the door to higher-level navigation applications. Future research will therefore focus on exploiting the estimated observables for precise positioning, as well as on extending the presented methods to multi-channel reception and multi-satellite scenarios.

ACKNOWLEDGEMENTS

The flexible front-end used within this work was developed within the project 'SeRANIS – Seamless Radio Access Networks for Internet of Space' funded by the dtec.bw – Digitalization and Technology Research Center of the Federal Armed Forces of Germany under Grant 150009910. The OFDM-tracking functionality and Matlab interface was developed within the project 'Forschungs- und Studienvorhaben für Innovation des Galileo GNSS-Systems (GalileoFUSION-II)' funded by the German Federal Ministry for Economic Affairs and Climate Action (BMWK) and administered by the Project Management Agency for Aeronautics Research of German Space Agency (DLR) in Bonn, Germany (grant no.50NA2301). The adaptions of the MuSNAT software receiver for transmitter identification, all real-world data recordings, and the dedicated receiver extension and analysis of specific signal was conducted within the project 'Hybrid PNT Study (HybPNT): LEO Constellations, 5G, HAPS and GNSS integration' funded by the European Commission under the contract number DEFIS/2022/OP/0009.

REFERENCES

3GPP (2022). Study on non-terrestrial networks (NTN). *3GPP Technical Report TR 38.811*.

Binder, F., Hameed, M. S., Lichtenberger, C. A., Picchi, O. M., Winkel, J., Rotoloni, M., and Soualle, F. (2026). Remarks on tracking 5G NTN signals with a GNSS-centric SDR: CRLB, GPU/CPU-based correlation and C/N_0-estimation. In *Proceedings of the 2026 International Technical Meeting of The Institute of Navigation (ITM)*, pages Session A2: Alternatives, Backups, Complements to GNSS 1, Anaheim, CA, USA. Institute of Navigation. Paper ID: 16343.

Humphreys, T. E., Iannucci, P. A., Komodromos, Z. M., and Graff, A. M. (2023). Signal structure of the Starlink Ku-band downlink. *IEEE Transactions on Aerospace and Electronic Systems*, 59(5):6016–6030.

Kassas, Z. M., Khalife, J., and Shamaei, K. (2018). Signals of opportunity for positioning and navigation. *IEEE Signal Processing Magazine*, 35(5):89–105.

Komodromos, Z. M. and Humphreys, T. E. (2025). Signal parameter estimation and demodulation of the OneWeb Ku-band downlink. To be published in journal.

Kozhaya, S., Saroufim, J., and Kassas, Z. M. (2024a). Characterization of carrier phase behavior in Starlink Ku-band signals. In *Proceedings of the IEEE International Conference on Wireless for Space and Extreme Environments (WiSEE)*.

Kozhaya, S., Saroufim, J., and Kassas, Z. M. (2024b). Opportunistic positioning with Starlink and OneWeb LEO Ku-band signals. In *2024 IEEE International Conference on Wireless for Space and Extreme Environments (WiSEE)*, pages 112–117.

Kozhaya, S., Saroufim, J., and Kassas, Z. Z. M. (2025). Unveiling Starlink for PNT. *NAVIGATION: Journal of the Institute of Navigation*, 72(1).

Lichtenberger, C. A., Arizabaleta, M., Binder, F., Soualle, F., and Pany, T. (2024). On the integration of tone-like signals-of-opportunity within a geodetic grade GNSS SDR. In *Proceedings of the 37th International Technical Meeting of the Satellite Division of The Institute of Navigation (ION GNSS+ 2024)*, GNSS 2024, page 3481–3497. Institute of Navigation.

Lichtenberger, C. A., Binder, F., Picchi, O. M., Menzione, F., and Pany, T. (2025). Using a block-processing discriminator for precise tracking of Starlink signals. In *ION GNSS+, The International Technical Meeting of the Satellite Division of The Institute of Navigation*, pages 3479–3491. Institute of Navigation.

Morton, Y. J. (2021). GNSS receiver signal tracking. In Morton, Y. T. J., van Diggelen, F., James J. Spilker, J., and Parkinson, B. W., editors, *Position, Navigation, and Timing Technologies in the 21st Century*, pages 339–375. IEEE Press, Wiley, Piscataway.

Pany, T. (2010). *Navigation Signal Processing for GNSS Software Receivers*. GNSS Technology and Applications. Artech House, Norwood, MA.

Pany, T., Euler, H.-G., and Winkel, J. (2012). Difference correlators: Does indoor carrier phase tracking allow indoor RTK? *insideGNSS*, 7(3):62–73.

Qin, W., Graff, A. M., Clements, Z. L., Komodromos, Z. M., and Humphreys, T. E. (2025). Timing properties of the Starlink Ku-band downlink.

Qin, W., Komodromos, Z. M., and Humphreys, T. E. (2024). An analysis of the short-term time stability of the starlink ku-band downlink frame clock. In *2024 IEEE International Conference on Wireless for Space and Extreme Environments (WiSEE)*, pages 106–111.

Roßbach, U. (2001). *Positioning and navigation using the Russian satellite system GLONASS*. Univ. der Bundeswehr München, Studiengang Geodäsie und Geoinformationen.

Soualle, F., Arizabaleta, M., Lichtenberger, C. A., Pany, T., del Peral-Rosado, J. A., De Vaucorbeil, X., Ligorio, G., Canzian, L., Rozzi, F., Rotoloni, M., Garlaschi, S., Menzione, F., Picchi, O., and Boyero, J. P. (2024). New generation of PNT user

terminals exploiting hybridization with LEO constellations. In *Proceedings of the 37th International Technical Meeting of the Satellite Division of The Institute of Navigation (ION GNSS+ 2024)*, GNSS 2024, page 887–947. Institute of Navigation.

Soualle, F., del Peral-Rosado, J. A., Ligorio, G., Al Faris, S., Binder, F., Lichtenberger, C. A., Pany, T., Winkel, J., Canzian, L., Rozzi, F., Rotoloni, M., Garlaschi, S., Castellan, G., Picchi, O. M., Menzione, F., and Boyero, J. P. (2025). Experimental framework for hybrid navigation terminals exploiting LEO PNT constellations. In *Proceedings of the 38th International Technical Meeting of the Satellite Division of The Institute of Navigation (ION GNSS+ 2025)*, GNSS 2025. Institute of Navigation.

Yang, S., Khodabandeh, A., Zaminpardaz, S., and Teunissen, P. J. G. (2025). Ambiguity-resolved short-baseline positioning performance of LEO frequency-varying carrier phase signals: a feasibility study. *J. Geod.*, 99(2).